

See discussions, stats, and author profiles for this publication at: <https://www.researchgate.net/publication/51466435>

Kinetically Controlled Seeded Growth Synthesis of Citrate-Stabilized Gold Nanoparticles of up to 200 nm: Size Focusing versus Ostwald Ripening

ARTICLE in LANGMUIR · JULY 2011

Impact Factor: 4.46 · DOI: 10.1021/la201938u · Source: PubMed

CITATIONS

185

READS

668

3 AUTHORS, INCLUDING:



Neus G Bastús

Catalan Institute of Nanoscience and Nanot...

36 PUBLICATIONS 1,237 CITATIONS

[SEE PROFILE](#)



Victor Puntes

Catalan Institute of Nanoscience and Nanot...

130 PUBLICATIONS 7,118 CITATIONS

[SEE PROFILE](#)

Kinetically Controlled Seeded Growth Synthesis of Citrate-Stabilized Gold Nanoparticles of up to 200 nm: Size Focusing versus Ostwald Ripening

Neus G. Bastús,^{*,†} Joan Comenge,^{†,‡,§} and Víctor Puntes^{*,†,§,||}

[†]Institut Català de Nanotecnologia (ICN), Campus UAB, 08193 Bellaterra, Barcelona, Spain

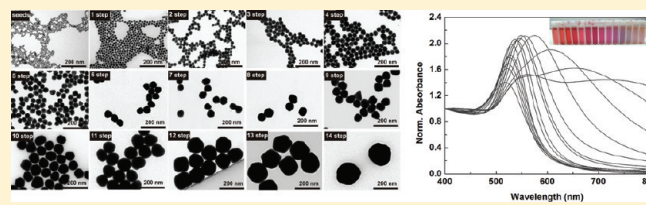
[‡]International Iberian Nanotechnology Laboratory (INL), Av. Central 100, 4710-229 Braga, Portugal

[§]Universitat Autònoma de Barcelona (UAB), Campus UAB, 08193 Bellaterra, Barcelona, Spain

^{||}Institut Català de Recerca i Estudis Avançats (ICREA), 08010 Barcelona, Spain

 Supporting Information

ABSTRACT: Monodisperse citrate-stabilized gold nanoparticles with a uniform quasi-spherical shape of up to ~ 200 nm and a narrow size distribution were synthesized following a kinetically controlled seeded growth strategy via the reduction of HAuCl_4 by sodium citrate. The inhibition of any secondary nucleation during homogeneous growth was controlled by adjusting the reaction conditions: temperature, gold precursor to seed particle concentration, and pH. This method presents improved results regarding the traditional Frens method in several aspects: (i) it produces particles of higher monodispersity; (ii) it allows better control of the gold nanoparticle size and size distribution; and (iii) it leads to higher concentrations. Gold nanoparticles synthesized following this method can be further functionalized with a wide variety of molecules, hence this method appears to be a promising candidate for application in the fields of biomedicine, photonics, and electronics, among others.



INTRODUCTION

Size and shape control of metal nanoparticles (NPs) has been the focus of continuous efforts during the past decades. In particular, Au NPs have been intensively studied because of their size- and shape-dependent physicochemical properties,¹ which are of enormous interest for applications in photonics, catalysis, electronics, and biomedicine.^{1,2} The synthesis of citrate-stabilized Au NPs based on the single-phase aqueous reduction of tetrachloroauric acid (HAuCl_4) by sodium citrate, initially developed by Turkevich et al.³ in 1951 and further refined by Frens et al.,⁴ still remains the most commonly employed aqueous method. Following this strategy, it is possible to control the size of Au NPs from 5 to 150 nm by simply varying the reaction conditions (sodium citrate to gold salt ratio,⁴ solution pH,⁵ and solvent⁶). However, the quality (size and size distribution) of the particles is quite poor, and the shapes obtained are nonuniform and irregular, such as quasi-spheres, ellipsoids, and triangles.⁷

Nowadays, seeding-mediated synthesis strategies based on the temporal separation of nucleation and growth processes are considered to be very efficient methods to control the Au NP size and shape precisely.^{8,9} Natan and co-workers pioneered the seeded growth of Au NPs using mild reducing agents such as sodium citrate¹⁰ or hydroxylamine^{11,12} to obtain Au NPs of up to 100 nm in diameter. Although the resultant NPs showed improved physical properties compared to those obtained by the citrate reduction of Au^{3+} (Frens method), its synthesis was

accompanied by a second population of rod-shaped particles. This work was further improved by Murphy¹³ and Liz-Marzan¹⁴ in reporting the synthesis of monodisperse Au NPs of up to ~ 180 nm in diameter using ascorbic acid as a reducing agent and cetyltrimethylammonium bromide (CTAB) as a cationic surfactant. Although CTAB-based methods allow the control of Au NP morphology, the use of molecules that strongly bind to the Au surface restricts the possibility of further functionalization because their replacement/displacement by thiols is difficult to achieve.¹⁵ This condition is especially important in biomedicine, where the ability to render a biological functionality to inorganic nanostructures is one of the cornerstones of this emerging field. In this context, citrate-stabilized Au NPs are unique candidates because the loosely bound capping layer provided by the sodium citrate can easily be exchanged by thiolated molecules that pseudocovalently bind (~ 45 kcal/mol) to the gold surface.¹⁶ In this way, Au NPs derived with proteins, peptides, antibodies, and thiolated DNA^{17–19} have been used in promising applications in the fields of diagnosis, therapy, delivering, and sensing, among others.²⁰

Therefore, the development of alternative routes leading to both high monodispersity and versatile surface chemistry still

Received: May 24, 2011

Revised: June 30, 2011

Published: July 05, 2011

remains a challenging task for Au NPs larger than 40 nm. In this context, several seed-mediated synthesis strategies, based on the use of 2-mercaptosuccinic acid²¹ or ascorbic acid²² as reducing agents in aqueous solvents, have been recently reported. In the first case, as when CTAB is used,^{13,14} the growth is controlled by the strongly binding surfactant molecules, which compromises further functionalization of the NPs. In the second case, Au NPs over a large range of sizes were grown by the incorporation of small gold clusters on the surfaces of seed particles. Further heat-mediated recrystallization led to quasi-spherical Au NPs via an interparticle ripening process. In this work, we study the conditions by which it is possible to obtain large, citrate-stabilized Au NPs via a seeded growth method whereas the new nucleation of particles is suppressed. This method allows better control of the final Au NP size and provides extremely stable and readily functionalized particles.

Herein, a seeded growth strategy for the synthesis of size- and shape-controlled large citrate-stabilized Au NPs based on the classical Turkevich/Frens reaction system is described. It focuses on the inhibition of secondary nucleation during the homogeneous growth process, allowing the enlargement of presynthesized Au NPs via the surface-catalyzed reduction of Au^{3+} by sodium citrate. The success of the method relies on the kinetic control of growth process by adjusting the reaction conditions, in detail, temperature, pH level, and seed concentration. It is noteworthy in several respects: (i) it produces particles of high monodispersity; (ii) it allows smaller particles to be grown into larger particles of a predetermined size; and (iii) it leads to higher Au NP concentrations relative to the Frens method (from 3×10^{12} NPs/mL, 8.5 nm to 5×10^9 NPs/mL, 180.5 nm). Additionally, it provides key aspects, identifying and explaining the important synthetic variables that must be controlled in order to control the Au NP morphology. Results show the reproducible preparation of citrate-stabilized Au NPs with a uniform quasi-spherical shape from 10 to ~ 180 nm, a narrow size distribution, and controlled concentration. These results allow the expansion of the well-known applicability of these NPs in biological and biomedical applications. Thus, large Au NPs arise as ideal candidates for biolabeling because of their higher electronic contrast.²⁰ Similarly, the intense visible absorption of larger Au NPs (which is translated into greatly enhanced local electromagnetic fields) promotes its use as surface-enhanced Raman spectroscopy (SERS) agents with superior activity.²³ The different accumulation/penetration behavior of Au NPs in tumors makes accurate control of the Au NP size necessary.²⁴ Moreover, the increase in the Au NP size (which entails a decrease in the radii of curvature) increases the number density of molecules that can be delivered. Additionally, the size-dependent biodistribution of Au NPs together with the elucidation of their potential toxicity,²⁵ usually related to the NP morphology, composition, or surface coating,²⁶ requires a wide catalog of NPs with controlled size and morphology and identical structure, composition, and surface chemistry. This method can be potentially adapted to continuous processes as in flow reactors, where the production of large numbers of particles of the highest quality is a limitation of Au NP technology implementation.

■ EXPERIMENTAL SECTION

Materials. $\text{HAuCl}_4 \cdot 3\text{H}_2\text{O}$ (99%) and trisodium citrate (99%) were purchased from Sigma-Aldrich. Milli-Q water was used in all

experiments. All glassware was cleaned with acetone, rinsed with deionized water, and stored at 150 °C before use.

Synthesis of Gold Nanoparticles. *Synthesis of Au Seeds.* A solution of 2.2 mM sodium citrate in Milli-Q water (150 mL) was heated with a heating mantle in a 250 mL three-necked round-bottomed flask for 15 min under vigorous stirring. A condenser was utilized to prevent the evaporation of the solvent. After boiling had commenced, 1 mL of HAuCl_4 (25 mM) was injected. The color of the solution changed from yellow to bluish gray and then to soft pink in 10 min. The resulting particles (~ 10 nm, $\sim 3 \times 10^{12}$ NPs/mL) are coated with negatively charged citrate ions and hence are well suspended in H_2O .

Seeded Growth of Au NPs of Up to 30 nm in Diameter. Immediately after the synthesis of the Au seeds and in the same vessel, the reaction was cooled until the temperature of the solution reached 90 °C. Then, 1 mL of sodium citrate (60 mM) and 1 mL of a HAuCl_4 solution (25 mM) were sequentially injected (time delay ~ 2 min). After 30 min, aliquots of 2 mL were extracted for further characterization by transmission electron microscopy (TEM) and UV-vis spectroscopy. By repeating this process (sequential addition of 1 mL of 60 mM sodium citrate and 1 mL of 25 mM HAuCl_4), up to 14 generations of gold particles of progressively larger sizes were grown (further details in Scheme S1). The concentration of each generation of NPs was approximately the same as the original seed particles ($\sim 3 \times 10^{12}$ NPs/mL).

Seeded Growth of Au NPs of Up to 180 nm in Diameter. Immediately after the synthesis of the Au seeds and in the same reaction vessel, the reaction was cooled until the temperature of the solution reached 90 °C. Then, 1 mL of a HAuCl_4 solution (25 mM) was injected. After 30 min, the reaction was finished. This process was repeated twice. After that, the sample was diluted by extracting 55 mL of sample and adding 53 mL of MQ water and 2 mL of 60 mM sodium citrate (further details in Scheme S2). This solution was then used as a seed solution, and the process was repeated again. By changing the volume extracted in each growth step, it is possible to tune the seed particle concentration.

Characterization Techniques. *UV–Vis Spectroscopy.* UV-visible spectra were acquired with a Shimadzu UV-2400 spectrophotometer. A Au NP solution (1 mL) was placed in a cell, and spectral analysis was performed in the 300 to 800 nm range at room temperature. In the case of time-dependent measures, aliquots of the solution were taken out and samples were cooled in ice water to quench the reaction.

Transmission Electron Microscopy. Gold nanoparticles were visualized using 80 keV TEM (JEOL 1010, Japan). Ten microliter droplets of the sample were drop casted onto a piece of ultrathin Formvar-coated 200-mesh copper grid (Ted-pella, Inc.) and left to dry in air. TEM images of the prepared colloidal Au NPs were used for the size distribution measurements. For each sample, the size of at least 100 particles was measured and the average size and the standard distribution were obtained.

Mie Calculations. Calculations of the scattering coefficient of colloidal Au NPs of different diameters were obtained using Mie plot software considering Au spheres embedded in water at 25 °C. In all cases, mean size and standard distribution measured by TEM were used for the calculations.

■ RESULTS

Seeded Growth Synthesis of Au NPs of Up to 30 nm. Gold seeds (~ 10 nm, $\sim 3 \times 10^{12}$ NPs/mL) were prepared by injecting an aqueous HAuCl_4 precursor solution into a boiling solution of sodium citrate (SC), and the reaction was run until it reached a red-wine color. After that, the temperature of the solution was decreased to 90 °C and more sodium citrate and HAuCl_4 precursor were injected. The decrease in the temperature to 90 °C allows both the inhibition of the new nucleation of Au NPs and the slowing down of the reaction, which helps in the

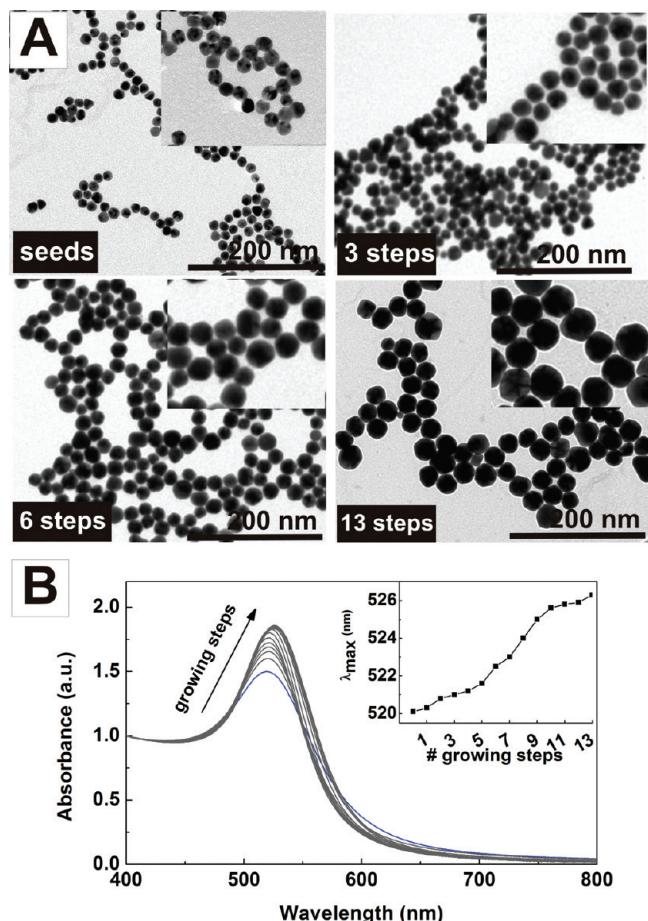


Figure 1. Seeded growth without the dilution of the seed solution. (A) Transmission electron microscopy images of Au seed particles and those obtained after different growth steps. The particle size increases from 13.5 ± 2.1 to 19.2 ± 2.6 , 24.8 ± 3.4 , and 30.5 ± 3.9 nm after 3, 6, and 13 growth steps, respectively. (B) Absorption spectra of gold colloids obtained after different growth steps and evolution of the SPR wavelength as a function of the growth step. All spectra are normalized at 400 nm to facilitate comparison.

monitoring of reaction kinetics and the delay of the defocusing period (vide infra). Figure 1A shows the morphological characterization of Au NPs obtained after different growth steps. As can be seen, the size of the Au NPs increased from 13.5 ± 2.1 to 30.5 ± 3.9 nm after 13 consecutive growth steps to obtain Au NPs with diameters of 19.2 ± 2.6 and 24.8 ± 3.4 nm after three and six growth steps, respectively (Figure S1). The optical properties of Au colloidal solutions measured by UV-vis spectroscopy are depicted in Figure 1B. Spectra were normalized to 400 nm, where the absorbance is mainly due to interband transitions, in order to facilitate a comparison.¹⁴ In all cases, the spectra show a rather symmetric surface plasmon absorption band, which red shifts (inset of Figure 1B) and increases in intensity as a consequence of particle growth. Interestingly, when comparing the size of the Au NP size measured from TEM images after different growth steps, it can be seen that the growth of the Au NPs is not homogeneous and decreases as the particle size increases. This is simply due to the fact that the rate of growth is determined by the relation between the diameter of the growing particle to the amount of gold added (considering a constant NP concentration).

Three different aspects are of crucial importance to obtaining Au NPs of large size and high stability: (i) the temperature of the solution, (ii) control of the pH of the solution, and (iii) the number of Au atoms injected in each growth step. First, because the kinetics of the gold reduction significantly depends on the temperature (Figure S2), we would expect that at low temperatures the nucleation rate decreases, leading to more favorable conditions for particle growth. Thus, the temperature was decreased to 90°C to prevent any secondary nucleation during the growth step. This assumption was experimentally confirmed by repeating the above-described experiment at 100°C . Whereas particles synthesized at 90°C presented excellent morphology and narrow size distributions, those obtained at 100°C (Figure S3) showed two different size populations, one of them smaller than the initial seed Au NPs. This indicates that secondary nucleation was not prevented. Another important aspect is the role of sodium citrate as a pH buffer in the reaction. Because each growth step involves the addition of a Au^{3+} precursor that acidifies the solution,⁵ the pH of the solution progressively decreases as the growth process is taking place. This was experimentally proven by repeating the reaction without the addition of sodium citrate and measuring the pH of the solution after each growth step (Figure S4). We found a decrease of 0.3 pH unit after each injection, achieving a value of 3.14 after 14 consecutive injections. At this point, the solution of Au NPs precipitated. This can be explained by considering the pK_a values of sodium citrate (6.4, 4.8, and 3.2). Because at pH 3.14 the protonation of all of the carboxylic groups occurred, the electrostatic interactions cannot impart stability to particles in solution. Thus, the amount of sodium citrate added in each growth step was the experimentally determined to maintain a constant pH of ~ 7 during the whole growth process. The last point to address is the amount of Au precursor added in each growth step. As previously discussed, the growth of the Au NPs is determined by the ratio between the gold atoms added and those present at the seed surface, which leads to a growth rate that drastically decreases as the particles become larger. This problem cannot be solved by injecting larger amounts of gold salt. The injection of larger amounts ($5\times$) broadens the size distribution, leading to nonspherical (oval) shapes probably because of the cementing of different seeds during the growth process,²⁷ whereas the injection of larger amounts ($10\times$) induces the nucleation of new Au NPs (Figure S5). In this context, we studied the possibility to decrease the seed particle concentration as NPs grew.

Seeded Growth Synthesis of Au NPs of Up to 180 nm. To get larger particles with a controlled size, morphology, and concentration, we studied the possibility to grow a successive generation of spherical particles with larger sizes by adjusting both the seed particle concentration and the total number of gold atoms injected into the solution. Thus, after two growth steps, Au seeds were diluted and more gold precursor and sodium citrate were added. By repeating this process, we synthesized Au NPs with increasing size and decreasing concentration. The morphology of the resultant Au NPs was determined by TEM microscopy. Figure 2 shows how the final size of the particles increases as the number of growth steps increases, and it is possible to synthesize spherical and monodisperse Au NPs of up to ~ 200 nm in diameter (Table 1). Consequently, the concentration of the colloidal gold solutions depends on the particle size. Thus, initial seed particles are present in a concentration of $\sim 3 \times 10^{12}$ NPs/mL but at $\sim 5 \times 10^9$ NPs/mL for the largest Au NPs. Moreover, although the particles are rather faceted and thus not

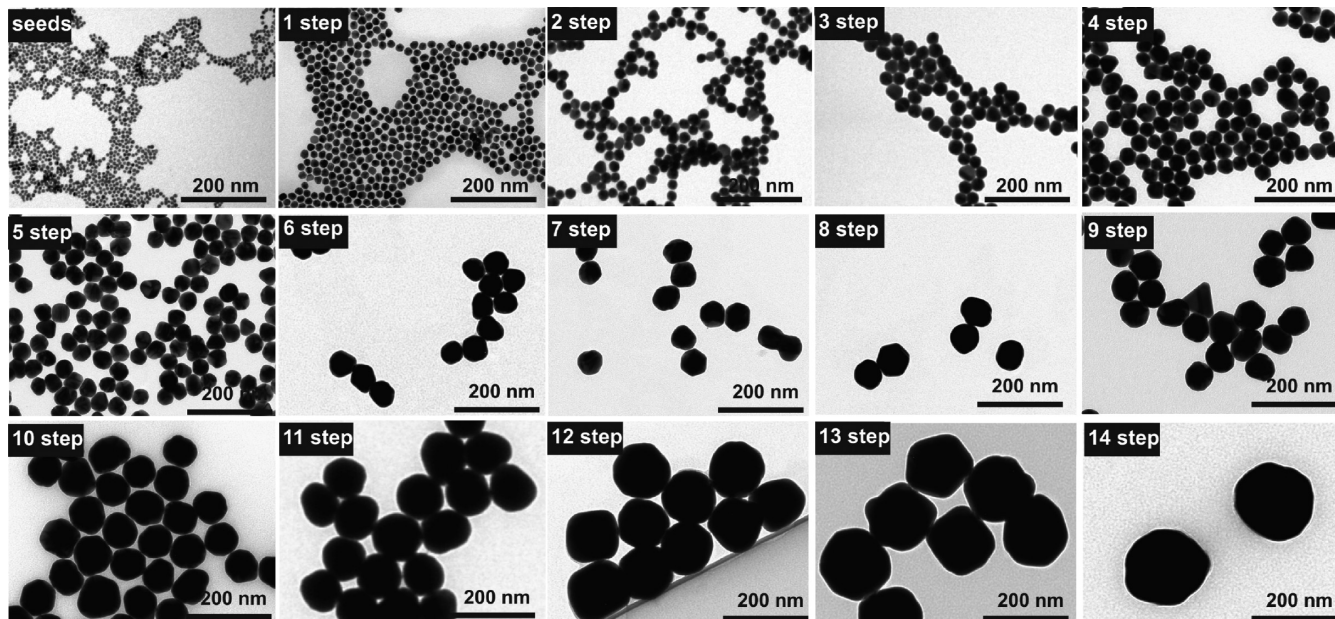


Figure 2. Seeded growth with the dilution of the seed solution. Transmission electron microscopy images of Au seed particles and those obtained after different growth steps. The particle size increases from 8.4 ± 1.0 to 180.5 ± 10.7 nm, and its concentration decreases from $\sim 3 \times 10^{12}$ to $\sim 5 \times 10^9$ NPs/mL.

Table 1. Summary of Sizes, Concentrations, and Optical Properties of the Au NPs Obtained after Different Growth Steps

growth step	diameter (nm)	SD (%)	concentration (NPs/mL)	SRP peak (dipolar) (nm)	SRP peak (quadrupolar) (nm)	expected diameter (nm)
seeds	8.4 ± 1.0	11.9	3.0×10^{12}	518		
1st	17.6 ± 1.2	6.8	1.9×10^{12}	521.5		18.2
2nd	22.3 ± 2.2	9.8	1.2×10^{12}	523.5		24.5
3rd	31.1 ± 2.8	9.0	7.6×10^{11}	525.5		30.4
4th	36.0 ± 2.4	6.6	4.8×10^{11}	527.5		36.7
5th	42.2 ± 2.3	7.8	3.1×10^{11}	530.5		43.7
6th	54.4 ± 3.3	6.1	1.9×10^{11}	535		51.5
7th	64.8 ± 3.4	5.2	1.2×10^{11}	540		60.5
8th	69.3 ± 4.5	6.5	7.8×10^{10}	542.5		70.7
9th	80.1 ± 5.4	6.7	4.9×10^{10}	546.5		82.6
10th	96.1 ± 5.6	5.8	3.1×10^{10}	555.5		96.4
11th	109.2 ± 7.6	6.9	2.0×10^{10}	574.5		112.4
12th	123.6 ± 10.6	8.6	1.2×10^{10}	606		131.0
13th	150.0 ± 9.9	6.6	7.9×10^9	649	545	152.6
14th	180.5 ± 10.7	5.9	5.0×10^9	720	560	177.8

perfectly spherical, the growth is very uniform up to ~ 180 nm without the formation of elongated particles or a second population of smaller particles (S6 and S7). The synthesis was finished when we achieved a particle size of ~ 180 nm as the colloidal transparency limit, but there is no reason against carrying out subsequent growth steps to achieve larger Au NPs.

Monitoring the Growth Process of the Gold Nanoparticles. To determine whether the growth of the Au NPs was via atom addition or the aggregation of smaller units forming compact aggregates,^{22,28} we monitored a single growth step by extracting different aliquots of the reaction after the initialization event (addition of Au^{3+} precursor to the seed NP solution). Several aliquots were taken at different reaction times and were immediately quenched by sample immersion in an ice/water

mixture for further TEM and UV-vis analysis. Evidence of Au NP growth can be seen from the UV-vis data (Figure 3), and two different behaviors can be observed. At short times (from 15 s to 6 min), a great red shift (from 524.5 to 532.5 nm) in the surface plasmon resonance (SPR) band position can be observed whereas absorbance values increased only slightly (from ~ 0.31 to ~ 0.48). At longer times (from 6 min on), a great increase in the absorbance (from ~ 0.48 to ~ 1.21) and a slight blue shift (from 532.5 to 529.5 nm) were observed. The same aliquots were analyzed by TEM. Initially, seed particles were 29.8 ± 3.3 nm in diameter, and they grew to 30.5 ± 3.5 nm (15 s), 32.2 ± 3.3 nm (30 s), 32.8 ± 3.3 nm (45 s) and 34.6 ± 3.8 nm (1 m). At these initial times, Au NPs were accompanied by aggregates (15 s) or small particles, which were not taken into account to calculate the

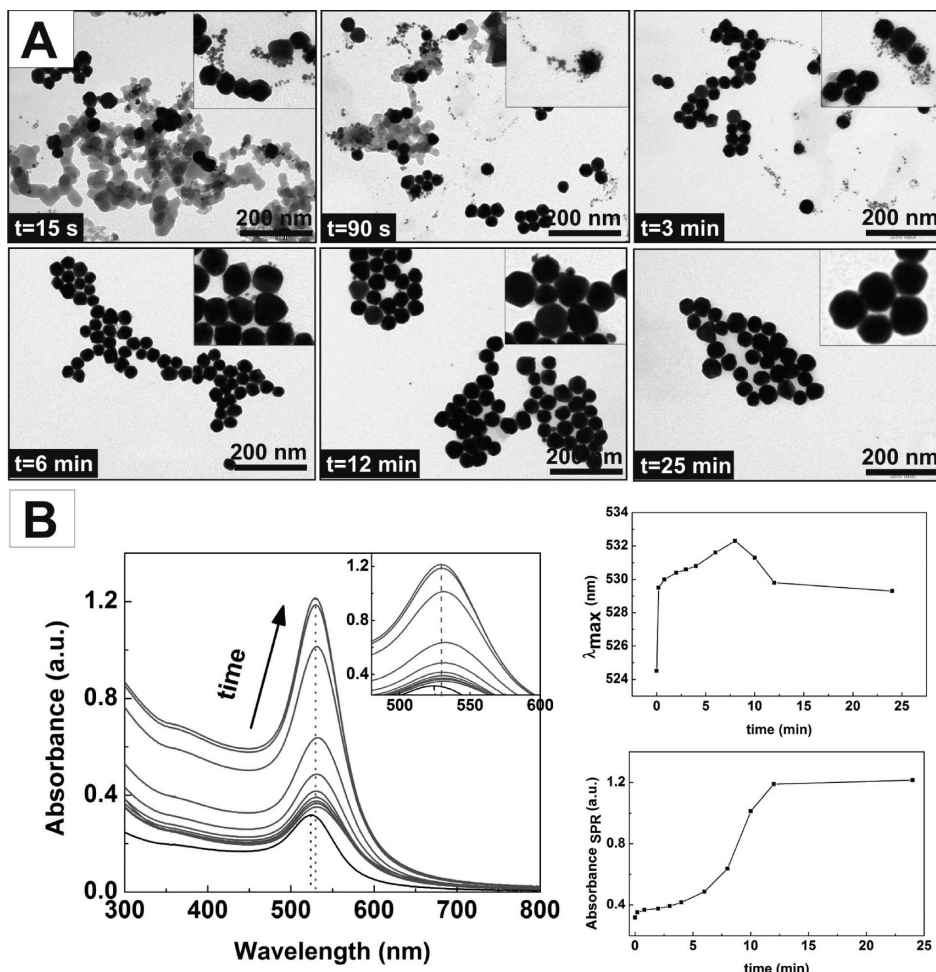


Figure 3. Temporal evolution of Au NP growth as a function of time. (A) Representative TEM images of Au NP growth at different times. Aggregates formation was observed at early stages (15 s) in which small particles formed (45 s) and then dissolved, acting as a source of atoms for the growth of large particles. (B) UV-vis spectra of Au NP growth. The increase in absorption at 400 nm together with the blue shift of the SPR indicates that particles grow atom by atom and hence are not formed by smaller aggregates.

size distribution because the small particles disappeared at later times and probably redissolved. After 6 min, no more aggregates were observed and the particle size increased up to 36.0 ± 3.7 nm (6 min), 38.1 ± 3.7 nm (8 min), 42.1 ± 4.1 nm (12 min), and 45.0 ± 4.4 nm (25 min). This gradual increase in the Au NP size suggests that resultant particles grew by the incorporation of Au atoms at the surface.

Effect of Seed Concentration. To study how seed concentration affects the final particle size, we grew Au NPs using different concentrations of seed particles (from $\sim 7.5 \times 10^{11}$ to $\sim 1.5 \times 10^{11}$ NPs/mL). In all cases, the initial Au seeds used were 17.0 ± 1.7 nm in diameter, the final volume of the solution was the same, and the amount of Au precursor added was kept constant. The average particle size and particle morphology were determined by TEM, where the mean particle size decreased as the seed concentration increased (Figure 4A, Figure S8). Thus, it is possible to achieve Au NPs from 23.3 ± 1.7 to 36.6 ± 4.3 nm in one step by diluting (from $\sim 7.5 \times 10^{11}$ to $\sim 1.5 \times 10^{11}$ NPs/mL) a solution of Au seed particles of a solution of 17.0 ± 1.7 nm. These results were corroborated by UV-vis spectroscopy, which shows how the band maximum red shifts from 521.5 to 526.5 nm as the concentration of seed particles decreases (Figure 4B).

However, when the concentration of Au NPs is too low (the ratio of the Au NP concentration to the quantity of gold precursor added exceed a certain value), the nucleation of new particles could not be avoided (Figure 4A, red arrows). It is interesting that this ratio depends, among others, on the temperature of the solution, hence it could be possible to control the growth of larger particles further by either decreasing the temperature of the solution and/or using a lower concentration of seed NPs.

Particle Size Determination. Assuming that (i) all of the gold precursor injected is consumed during the reaction, (ii) particles are spherical in shape, and (iii) reduction and growth take place without further nucleation, the size of the grown particles can be quantitatively predicted using the following expression

$$r_{\text{AuNP}}^3 = r_{\text{seed}}^3 + \frac{3}{4} \frac{m_{\text{Au}}}{\pi \rho_{\text{Au}} n_{\text{seed}}}$$

where m_{Au} , n_{seed} , and ρ_{Au} are the Au mass added, the number of seed particles, and the gold density, respectively.

Figure 5 shows the theoretical curve of Au NP diameter for the different conditions used in each experiment: (i) the direct addition of Au precursor (Figure 1), (ii) the combined approach (Figure 2), and (iii) the dilution of Au seeds in a single growth

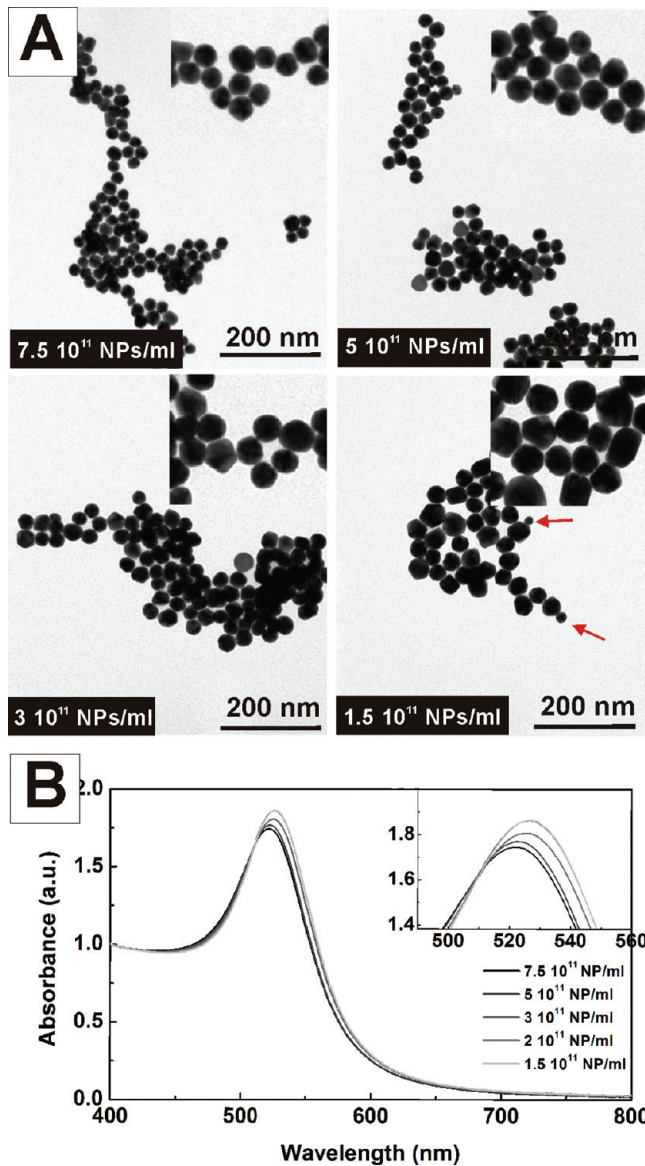


Figure 4. Effect of seed concentration. (A) Transmission electron microscopy images of Au particles obtained using different concentrations of seed while keeping the amount of Au precursor added constant. The final particle size depends on the seed concentration used, obtaining values of 23.3 ± 1.7 nm (7.5×10^{11} NPs/mL), 25.6 ± 2.6 nm (5×10^{11} NPs/mL), 29.2 ± 3.0 nm (3×10^{11} NPs/mL), and 36.6 ± 4.3 nm (1.5×10^{11} NPs/mL). The nucleation of a new population of particles appeared at low ratios of Au precursor to Au seeds (red arrows). Au seeds used were 17.0 ± 1.7 nm in diameter. (B) Absorption spectra of gold colloids obtained at different concentrations. All spectra all normalized at 400 nm to facilitate comparison.

step (Figure 4). As can be seen, in all cases the expected results fit with those obtained experimentally.

Optical Properties of Gold Nanoparticles. The optical properties of the different generation of Au NP solutions depicted in Figure 2 were measured by UV-vis spectroscopy (Figure 6A), where the observed trend agrees very well with the expected changes in the optical behavior for increasing particle size.¹⁴ The initial red shift from 518.5 to 556 nm as the size of the Au NPs increases from 8.4 to 96.1 nm confirms the Au NP growth. Moreover, considering that the elongated oval shape of

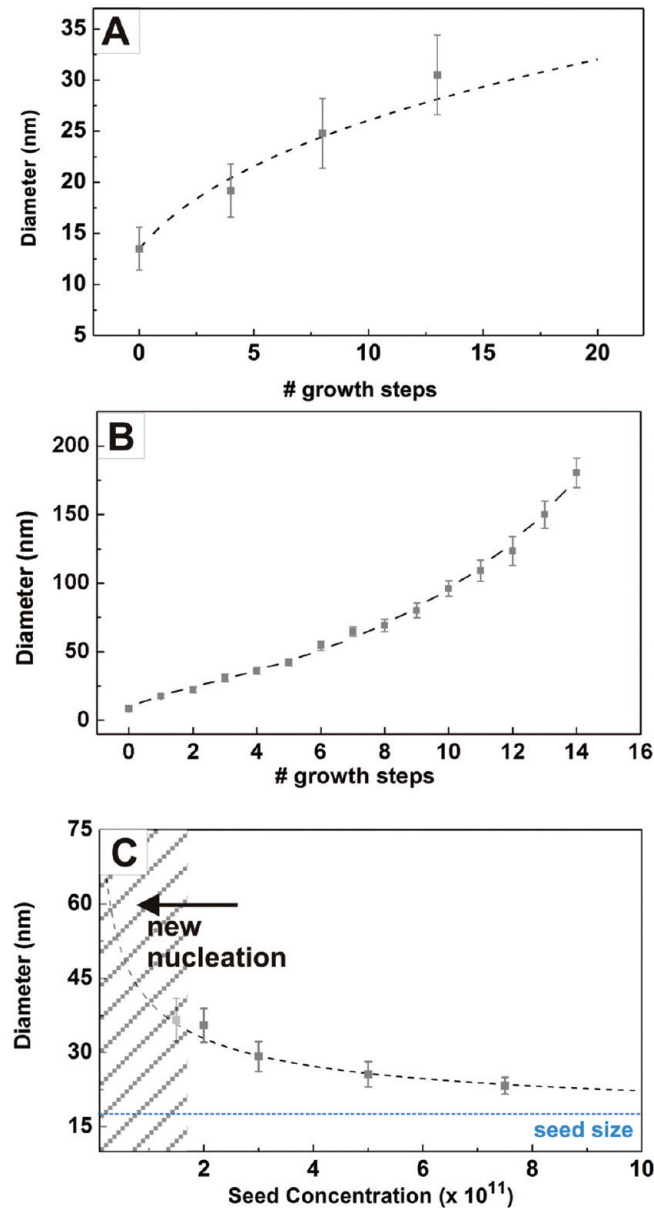


Figure 5. Average diameter of Au NPs and comparison with the expected results. Comparison of the theoretical curve (---) and experimental data for different experiments: (A) seeded growth without a dilution of the seed solution, (B) seeded growth with a dilution of the seed solution, and (C) the effect of the seed concentration. The blue line corresponds to the size of the initial seed Au NPs used. In all cases, the obtained results fit with those calculated, which indicates that no new nucleation occurred and that the Au atoms deposit onto the surfaces of the preformed particles.

Au NPs obtained by the Frens method is usually characterized by a nonzero extinction baseline at longer wavelength and a notable band asymmetry;⁵ these results are a further indication that Au NPs are monodisperse and quasi-spherical in shape. When the Au NP diameter further increases, the main dipolar resonance band red shifts and broadens, peaking at 574.5 nm for Au NPs with an average diameter of 109.2 nm. Interestingly, above 120 nm, the single band is accompanied by a shoulder at lower wavelengths, corresponding to a quadrupolar resonance placed at 560 nm for 180.5 nm Au NPs. The experimental absorbance

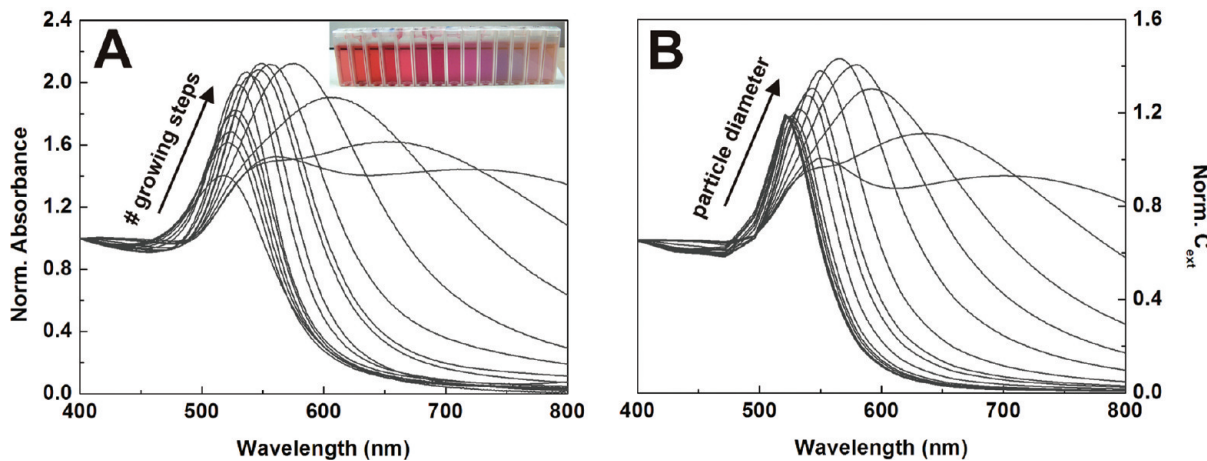
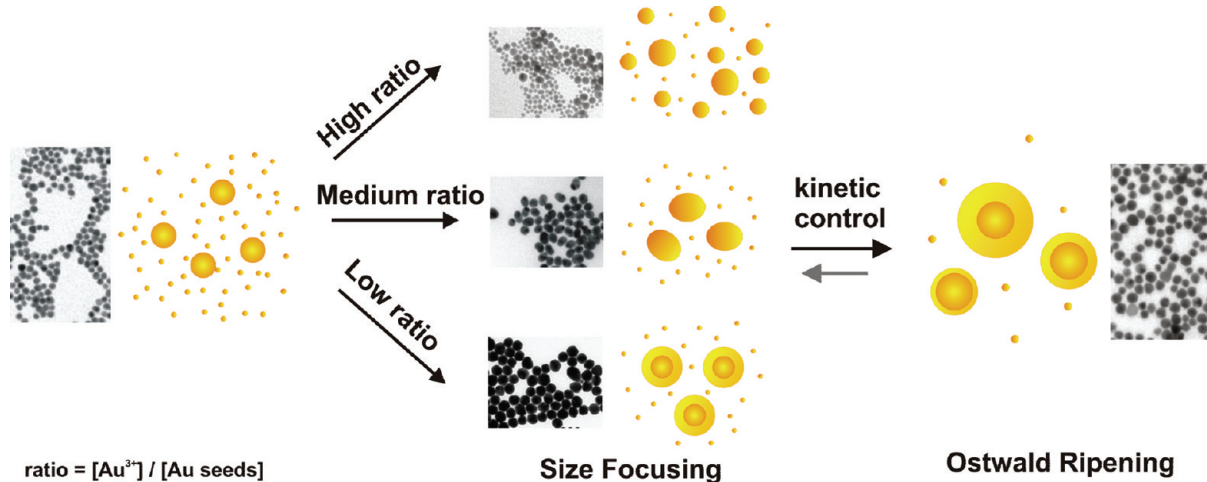


Figure 6. Seeded growth with the dilution of the seed solution. (A) UV-vis spectra of Au colloids obtained after different growth steps and (B) calculated extinction spectra of Au spheres with the same mean size and size distribution as obtained experimentally. All spectra all normalized at 400 nm to facilitate comparison.

Scheme 1. Illustration of the Different Growth Pathways for the Kinetically Controlled Seeded Growth of Au NPs^a



^a Control of the temperature of the solution together with the use of a low gold precursor to seed particle ratio allows us to shift the equilibrium towards the size-focusing period. The addition of higher quantities of the gold precursor leads either to the formation of oval-shaped particles or to the new nucleation of smaller Au NPs.

data can be easily compared to calculations based on the standard Mie theory of spherical particles. Figure 6B plots the extinction spectra (containing both absorption and scattering contributions) calculated for Au spheres, with the average size and standard distribution measured from TEM images of each experimental sample using MiePlot software. Results obtained for large particles (>50 nm) are in full agreement with those that are experimentally measured. In fact, they are better than expected considering the small deviation from the spherical shape observed in the TEM images. This is a further indication that secondary nucleation occurred and that gold precursor deposited onto existing Au NPs, increasing their size. Significant differences were found in the case of small (<50 nm) Au NPs, where Mie theory fails to explain theoretically the size dependence of the surface plasmon absorption band. Although this problem can be solved by assuming a size-dependent Au NP dielectric function, these modifications are beyond the scope of this work and are reported elsewhere.^{29,30}

■ DISCUSSION

According to the LaMer mechanism,^{31,32} the growth process of NPs involves two different periods: (i) the focusing period, where the mean radius of the particles increases rapidly and the size distribution becomes narrower and (ii) the defocusing period, where the growth rates declines sharply and the size distributions broadens. This period, known as Ostwald ripening, is characterized by the growth of large particles that receive the atoms from the smaller dissolving particles. The switching point of these two different periods depends, among others, on the monomer concentration (Scheme 1). Thus, whereas at relatively high monomer concentrations the smaller NPs in the distribution grow faster than the larger ones (focusing), when the monomer concentration is depleted by growth, the distribution broadens because some smaller NPs shrinking and eventually disappear (Ostwald ripening).

In this scenario, it is possible to refocus the size distribution of the NPs by modifying the kinetics of the reaction³³ such as by

decreasing the temperature of the solution and/or injecting additional monomer. Therefore, by performing the synthesis reaction at lower temperatures, it is possible not only to prevent the nucleation of new NPs but also to delay the defocusing period. This was experimentally measured, where the time needed to reach the defocusing period depends on the temperature of the solution, in detail at 90 min and 100 °C and at more than 3 h and 90 °C. However, the injection of more gold precursor favors the focusing period to be maintained for a large mean radius, which leads to the controlled growth of the Au NPs. This correlates with the size distribution of the Au NPs, which is focused from 11.9 to 5.9% as the mean diameter increases from 8.4 to 180.5 nm, respectively. Additionally, considering that each growth step needs more than 45 min to finish, the diffusion of the gold monomer from smaller particles to larger ones would take place if the concentration of monomer would not increase. However, although the addition of more monomer allows the movement of the system toward the focusing conditions, it should be kept below the supersaturation value; otherwise, the new nucleation of Au NPs and/or the appearance of oval-shaped particles occurs. In this context, the control of the ratio between the number of Au seeds and the amount of gold monomer injected (Au NPs/Au³⁺) allows the growth of Au NPs in each growth step.

CONCLUSIONS

We report a general seeded growth route to synthesize large, monodisperse citrate-stabilized Au NPs through kinetic control of the reaction conditions. Three different aspects are of crucial importance in obtaining Au NPs with large sizes and high stability. The decrease in the temperature of the solution allows the slowing of the reaction and prevents any secondary nucleation. The control of the reaction pH allows control of the reactivity of the gold species, which has been proven to be an important point in improving the monodispersity of the resultant particles. Finally, the number of Au atoms injected in each growth step allows the shifting of the system towards the focusing conditions, which narrows the Au NP final distributions. As a consequence, Au NPs with diameters of up to ~200 nm have been synthesized. The ability to synthesize citrate-stabilized Au NP sizes from 10 to 200 nm with a controlled concentration and surface state allows the expansion of the well-known applicability of these NPs to biological and biomedical applications. In detail, the further functionalization with a wide variety of biologically active molecules, such as peptides, antibodies, and DNA allows their use as drug-delivery carriers, local and remote energy sources, and surface-enhanced Raman spectroscopy (SERS) platforms. Additionally, they can be used as model NP systems for toxicity studies and to elucidate the impact of NP morphology on biological systems.

ASSOCIATED CONTENT

S Supporting Information. Sample characterization (size distribution and TEM) and additional results. This material is available free of charge via the Internet at <http://pubs.acs.org>.

AUTHOR INFORMATION

Corresponding Author

*E-mail: neus.bastus@icn.cat, victor.puntes.icn@uab.es.

ACKNOWLEDGMENT

This work was supported by the Spanish Science Ministry (MAT2009-14734-C02-01). We thank Dr. Isaac Ojea-Jimenez for his critical reading of the manuscript.

REFERENCES

- (1) Sardar, R.; Funston, A. M.; Mulvaney, P.; Murray, R. W. *Langmuir* **2009**, *25*, 13840–13851.
- (2) Daniel, M.-C.; Astruc, D. *Chem. Rev.* **2003**, *104*, 293–346.
- (3) Turkevich, J.; Stevenson, P. C.; Hillier, J. *Discuss. Faraday Soc.* **1951**, *55*.
- (4) Frens, G. *Nature, Phys. Sci.* **1973**, *241*, 20–22.
- (5) Ji, X.; Song, X.; Li, J.; Bai, Y.; Yang, W.; Peng, X. *J. Am. Chem. Soc.* **2007**, *129*, 13939–13948.
- (6) Ojea-Jimenez, I.; Romero, F. M.; Bastús, N. G.; Puntes, V. *J. Phys. Chem. C* **2010**, *114*, 1800–1804.
- (7) Kimling, J.; Maier, M.; Okenve, B.; Kotaidis, V.; Ballot, H.; Plech, A. *J. Phys. Chem. B* **2006**, *110*, 15700–15707.
- (8) Perrault, S. D.; Chan, W. C. W. *J. Am. Chem. Soc.* **2009**, *131*, 17042–17043.
- (9) Bigall, N. C.; Halrtling, T.; Klose, M.; Simon, P.; Eng, L. M.; Eychmuller, A. *Nano Lett.* **2008**, *8*, 4588–4592.
- (10) Brown, K. R.; Walter, D. G.; Natan, M. J. *Chem. Mater.* **1999**, *12*, 306–313.
- (11) Brown, K. R.; Lyon, L. A.; Fox, A. P.; Reiss, B. D.; Natan, M. J. *Chem. Mater.* **1999**, *12*, 314–323.
- (12) Brown, K. R.; Natan, M. J. *Langmuir* **1998**, *14*, 726–728.
- (13) Jana, N. R.; Gearheart, L.; Murphy, C. J. *Langmuir* **2001**, *17*, 6782–6786.
- (14) Rodriguez-Fernandez, J.; Perez-Juste, J.; Garcia de Abajo, F. J.; Liz-Marzan, L. M. *Langmuir* **2006**, *22*, 7007–7010.
- (15) Leonov, A. P.; Zheng, J.; Clogston, J. D.; Stern, S. T.; Patri, A. K.; Wei, A. *ACS Nano* **2008**, *2*, 2481–2488.
- (16) Sellers, H.; Ulman, A.; Shnidman, Y.; Eilers, J. E. *J. Am. Chem. Soc.* **1993**, *115*, 9389–9401.
- (17) Bastús, N. G.; Sanchez-Tillo, E.; Pujals, S.; Farrera, C.; Lopez, C.; Giralt, E.; Celada, A.; Lloberas, J.; Puntes, V. *ACS Nano* **2009**, *3*, 1335–1344.
- (18) Niemeyer, C. M. *Angew. Chem., Int. Ed.* **2001**, *40*, 4128–4158.
- (19) Pujals, S.; Bastús, N. G.; Pereiro, E.; López-Iglesias, C.; Puntes, V. F.; Kogan, M. J.; Giralt, E. *ChemBioChem* **2009**, *10*, 1025–1031.
- (20) Sperling, R. A.; Gil, P. R.; Zhang, F.; Zanella, M.; Parak, W. J. *Chem. Soc. Rev.* **2008**, *37*, 1896–1908.
- (21) Niu, J.; Zhu, T.; Liu, Z. *Nanotechnology* **2007**, *18*, 325607.
- (22) Ziegler, C.; Eychmüller, A. *J. Phys. Chem. C* **2011**, *115*, 4502–4506.
- (23) Alvarez-Puebla, R. A.; Liz-Marzán, L. M. *Small* **2010**, *6*, 604–610.
- (24) Perrault, S. D.; Walkey, C.; Jennings, T.; Fischer, H. C.; Chan, W. *Nano Lett.* **2009**, *9*, 1909–1915.
- (25) Casals, E.; Vázquez-Campos, S.; Bastús, N. G.; Puntes, V. *Trends Anal. Chem.* **2008**, *27*, 672–683.
- (26) Chithrani, B. D.; Ghazani, A. A.; Chan, W. C. W. *Nano Lett.* **2006**, *6*, 662–668.
- (27) Lim, S. I.; Ojea-Jimenez, I.; Varon, M.; Casals, E.; Arbiol, J.; Puntes, V. *Nano Lett.* **2010**, *10*, 964–973.
- (28) Goia, D.; Matijevic, E. *New J. Chem.* **1998**, *22*, 1203–1215.
- (29) Kelly, K. L.; Coronado, E.; Zhao, L. L.; Schatz, G. C. *J. Phys. Chem. B* **2002**, *107*, 668–677.
- (30) Zhao, J.; Pinchuk, A. O.; McMahon, J. M.; Li, S.; Ausman, L. K.; Atkinson, A. L.; Schatz, G. C. *Acc. Chem. Res.* **2008**, *41*, 1710–1720.
- (31) Lamer, V. K.; Dinegar, R. H. *J. Am. Chem. Soc.* **1950**, *72*, 4847–4854.
- (32) Reiss, H. *J. Chem. Phys.* **1951**, *19*, 482–487.
- (33) Peng, X.; Wickham, J.; Alivisatos, A. P. *J. Am. Chem. Soc.* **1998**, *120*, 5343–5344.